nature photonics

ARTICLES

https://doi.org/10.1038/s41566-019-0370-1

Light guiding by artificial gauge fields

Yaakov Lumer[1,3], Miguel A. Bandres[1,3], Matthias Heinrich[2], Lukas J. Maczewsky[2], Hanan Herzig-Sheinfux[1], Alexander Szameit[2] and Mordechai Segev[1]*

Artificial gauge fields enable uncharged particles to behave as if affected by external fields. Generated by geometry or modulation, artificial gauge fields are instrumental in realizing topological physics in photonics, cold atoms and acoustics. Here, we experimentally demonstrate waveguiding by artificial gauge fields. We construct artificial gauge fields by using waveguide arrays with non-trivial trajectories. Tilting the arrays results in gauge fields that are different in the core and cladding, shifting their dispersion curves, thereby confining the light to the core. In a more advanced setting, we demonstrate waveguiding in a medium with the same gauge and dispersion everywhere, where the only difference between the core and the cladding is a phase shift in the dynamics of the gauge fields, which facilitates waveguiding via bound states in the continuum. Waveguiding and bound states in the continuum via artificial gauge fields relate to a plethora of systems, ranging from photonics and microwaves to cold atoms and acoustics.

Waveguiding—the ability to confine light in a region and guide it within a structure—is a fundamental building block in many photonics applications. The basic structure of a waveguide consists of a core region where the light is confined and a cladding region within which the core is embedded. Standard waveguide structures rely either on total internal reflection and are made up of a high-refractive-index core surrounded by a low-refractive-index cladding, or on metallic pipes where the electromagnetic fields are completely forbidden from escaping[1]. Other schemes rely on photonic systems with bandgaps[2–6], coupled resonator arrays[7], grating-mediated waveguiding[8], Kapitza-effect arrangements[9] or exploit the vectorial spin–orbit interaction of light in an anisotropic medium[10]. In all of these, the core and cladding are made from media with different dispersion relations. Recently, a conceptually new waveguiding mechanics was proposed, where the cladding and core region of a waveguide have the same dispersion curve, but the core's dispersion is shifted by virtue of an artificial gauge field[11].

Gauge fields are a fundamental concept in physics, describing the basic interactions between charged particles. Neutral particles (such as photons) are thus decoupled from real gauge fields. However, by properly engineering a physical system, one can generate artificial gauge fields that will govern the effective dynamics of neutral particles. An artificial gauge field can often be induced through the geometric design of a system or through some specific external modulation, such that the effective dynamics of the system behaves as if it were governed by a real gauge field. Artificial gauge fields play a crucial role in physics, because they allow us to endow systems with a wide range of intriguing features that are naturally not expected in them. Fundamentally, this opens the door to explore new physics, and from an applications point of view it facilitates new devices by enabling control over the dynamics of systems in new ways. For example, in cold neutral atoms it has been demonstrated that a synthetic magnetic field can be induced by rotating the system[12] or by judicious optical coupling between the internal states of the atoms[13]. Furthermore, artificial gauge fields have made it possible to explore topological phenomena outside the context of electronic systems, in photonics[14–16], ultracold atoms[17,18], optomechanical systems[19] and even in acoustic[20,21] and mechanical systems[22,23]. This is important, because bringing topological protection to virtually all wave systems opens the door to a wealth of applications never envisioned before.

In photonic systems specifically, artificial gauge fields have been proposed and demonstrated to induce dynamics that would otherwise be inconceivable for light. For example, artificial gauge fields were proposed in coupled resonators schemes as a means to realize wave dynamics under an effective magnetic field[24–27]. Numerous experiments followed, ranging from the induction of a strong effective magnetic field by spatially ordering waveguide arrays[28] and the creation of synthetic electric fields by making the waveguides helical—as was used to create photonic Floquet topological insulators[14]—to specifically designed bi-anisotropic photonic crystals that give rise to topologically robust propagation[29]. In a similar vein, dynamic localization[30–34] and Aharonov–Bohm phases have been demonstrated[35], as well as non-reciprocal devices using temporally modulated silicon photonics[36]. In this spirit of exploiting artificial gauge fields, novel optical devices have been proposed such as one-way mirrors, negative refraction and highly efficient mode convertors[37,38]. Finally, the concept of artificial gauge fields was introduced to active (non-Hermitian) systems, as highlighted by the recent observation of topological insulator lasers[39,40].

Recently, the use of artificial gauge fields to induce a fundamentally new kind of waveguiding mechanism was proposed[11]. The proposed structure consists of core and cladding regions that have the same underlying dispersion relation, but are subject to different artificial gauge fields, which in turn shift their dispersion relation with respect to one another. This shift between the dispersion curves in different regions makes it possible to design a structure where the core supports guided modes that do not have matching propagating states in the cladding region. Thus, the wavefunctions of these modes decay exponentially in the cladding regions, while being oscillatory in the core, as guided modes always are. To implement this idea, it was proposed to use arrays of resonators with temporal modulations of the refractive index at different sites. However, thus far, the concept of guiding light with artificial gauge fields has never been demonstrated in experiments.

Here, we present an experimental realization of waveguiding by artificial gauge fields. We implement this idea in an array of evanescently coupled identical waveguides, where the waveguides in the

[1]Physics Department and the Solid State Institute, Technion – Israel Institute of Technology, Haifa, Israel. [2]Institut für Physik, Universität Rostock, Rostock, Germany. [3]These authors contributed equally: Yaakov Lumer, Miguel A. Bandres. *e-mail: msegev@technion.ac.il

core and cladding follow different trajectories during propagation. In our system the artificial gauge field stems solely from the trajectory of the waveguides, and does not require external modulation of the material properties. Specifically, we present—theoretically and experimentally—two mechanisms for waveguiding with artificial gauge fields. In our first realization, the dispersion relations in the core and in the cladding are shifted from one another in momentum-space because of the artificial gauge field. This engineered dispersion relation creates propagating modes that are confined to the core only in specific ranges of transverse momenta. Our second realization is even more intriguing: the system is made not only of the same material, but also has the same artificial gauge field, such that the core and cladding have exactly the same dispersion relation. In that system, we induce guiding strictly by introducing a phase shift between the dynamics of the gauge fields at the core and at the cladding. We find that this system exhibits leaky modes for all values of transverse momentum, except for a specific value where perfect core confinement is obtained. This specific value can be controlled by the system parameters—that is, the waveguide trajectories. We show that this effect constitutes a dynamic bound state in the continuum (BIC)[41–45]. Thus, our experiments are in fact the first observation of dynamic BIC ever. Altogether, the ideas demonstrated here in our photonic platform can be implemented in other physical systems—such as ultracold atom systems, mechanical and acoustic systems—thereby enabling novel types of physical configuration, such as waveguides, couplers and photonic networks, in previously unconceived scenarios.

Waveguiding of light by artificial gauge fields

We begin by describing our system—a photonic lattice of evanescently coupled waveguides. The propagation of light in this structure is described by the paraxial wave equation

$$i\partial_z\psi(\mathbf{r}) = -\frac{1}{2k_0}\nabla_\perp^2\psi(\mathbf{r}) - \frac{k_0}{n_0}\Delta n(\mathbf{r})\psi(\mathbf{r}) \quad (1)$$

where ψ is the envelope of the electric field, k_0 is the wavenumber in the bulk material, n_0 is the ambient refractive index, $\nabla_\perp^2 = \partial_x^2 + \partial_y^2$ and $\Delta n(\mathbf{r}) = n(\mathbf{r}) - n_0$ comprise the relative refractive index profile. Our basic building block is a one dimensional array of evanescently coupled waveguides, which means that $\Delta n(\mathbf{r})$ is a periodic function in x with period d_x such that each period consists of a single waveguide. Using a coupled mode theory approach[46,47], we can show that the spectrum of such an array is $\beta = 2c_1\cos(k_x d_x)$ where k_x is the spatial momentum in the x direction and c_1 is the coupling strength between neighbouring waveguides (taken to be a positive number). Here, we define the propagation constant β by the ansatz $\psi(x,y,z) = \psi_0(x,y)e^{i\beta z}$. Tilting the array at an angle η makes the waveguides follow the trajectory $x - \eta z = \text{const}$. The spectrum of such a tilted array is given by[47]

$$\beta(k_x) = 2c_1\cos((k_x + k_0\eta)d_x) + \eta k_x \quad (2)$$

We notice that the tilting of the waveguides has two effects. First, the shift of $k_0\eta$ in k_x results from the constant tilt of the waveguides, and constitutes a type of Gallilean transformation. Second, the shift of ηk_x in the spectrum results from the fact that there is an angle between the z axis and the axis of the waveguides. Looking at equation (2), we can treat the tilt of the array as the effect of an artificial gauge field that depends on the tilting angle η. When we generalize and consider a two-dimensional array of waveguides, all tilted at the same angle η, we can treat our system as being subjected to a uniform gauge field. Such a uniform tilt would constitute a trivial gauge, that is, a trivial change of reference frame for the entire system, which can be readily gauged away. To generate a non-trivial gauge field, we couple arrays that have different tilting angles. In such a system, the gauge field becomes space-dependent and non-trivial; that is, there is no reference frame in which both arrays are not tilted. More importantly, the band structures of two arrays of different tilt angles are not the same due to the different gauge field, even though the arrays are identical up to a tilt. In this way, by modifying the band structures of the arrays by means of artificial gauge fields, we can now design a structure that exhibits guiding of light by virtue of an artificial gauge field, in the spirit of Lin and Fan[11].

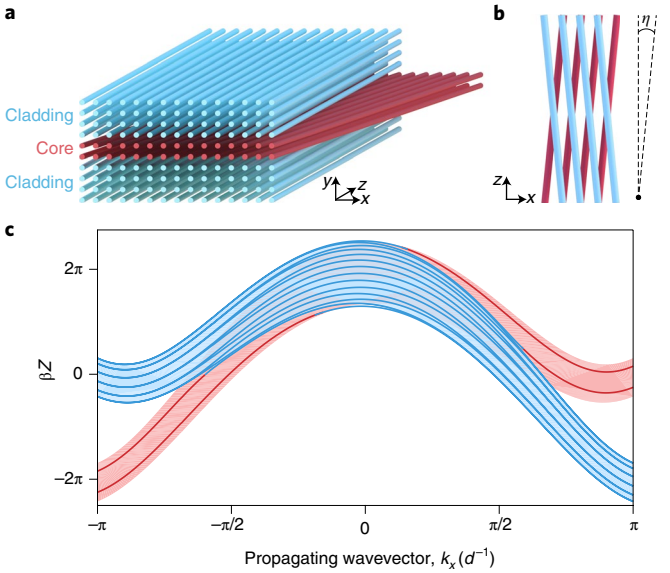

Fig. 1 | Waveguiding of light by artificial gauge fields in tilted arrays. **a**,**b**, Schematic of the two-dimensional waveguide array displaying waveguiding by an artificial gauge field. Cladding rows (blue) are tilted to the left and core rows (red), located at the centre, are tilted to the right. The tilt angle ($\pm\eta$) introduces an artificial gauge field, which is different for the core and cladding regions. **c**, Dispersion relation of the waveguide array in **a**. The blue shaded section represents the dispersion of just the cladding modes (all the arrays tilted by $-\eta$) and the red shaded section represents the dispersion assuming all the arrays are tilted at $+\eta$. Solid blue lines represent modes associated with the whole array (core + cladding) and red lines represent the two modes confined to the core. The distances between the waveguides are $d_x = 16\,\mu\text{m}$ and $d_y = 22\,\mu\text{m}$, the tilting angle is $\eta = \pm 8\,\mu\text{m}\,\text{cm}^{-1}$. The spectrum is calculated using $\lambda = 633\,\text{nm}$.

Consider a two-dimensional array of evanescently coupled waveguides, with the middle rows acting as the core and the remainder acting as the cladding, as depicted in Fig. 1a,b. The rows of waveguides in the core and the cladding are identical in every parameter (refractive index, waveguide shape, distance between the waveguides), except the tilting angle; the core is tilted at an angle of $+\eta$ and the cladding is tilted at an angle of $-\eta$ (Fig. 1b). Thus, the core and the cladding regions are subjected to different artificial gauge fields. Notice that the gauge field is non-trivial, as the gauge field gradient, specifically at the interface region, cannot be gauged away by a change of reference frame. Thus, although our system is still periodic in x with period d_x, it is no longer z-independent; rather, it is periodic in z with period $Z = d_x/\eta$. We calculate the spectrum of this photonic lattice (Fig. 1a) by Floquet diagonalization of the continuous paraxial equation (equation (1))[47]; this can also be calculated using an approximate tight-binding model[47]. The spectrum is presented in Fig. 1c. One immediately notes that the spectrum is not symmetric with respect to k_x, a fact that stems directly from the $z \to -z$ parity symmetry breaking of the underlying structure by virtue of the artificial gauge field. The asymmetric dispersion shown

here is similar to systems where time-reversal symmetry is broken by an actual magnetic field[48,49]. The Floquet analysis generates replicas that in general may overlap in the bandstructure. In our case, the Floquet periodicity in the spectrum is $\Omega = 2\pi/Z = 2\pi\eta/d_x$, which causes the replicas to overlap around $|k_x| = \pi$ (see Supplementary Information). However, our system has an additional glide symmetry—a translation of $Z/2$ along z causes the system to repeat itself up to a shift of $d_x/2$ along x. As shown in the Supplementary Information, this symmetry means that the true Floquet spectral period of the system is in fact double and equal to $4\pi\eta/d_x$, and the replicas in the band structure never overlap. In light of this, we present only one Floquet replica in the bandstructure shown in Fig. 1c.

Let us now analyse the spectrum (Fig. 1c) of our photonic lattice in detail. For reference, we also plot in Fig. 1c the dispersion relation of a two-dimensional array with all the waveguides tilted at the same angle as the core waveguides ($+\eta$; red shaded region) and as the cladding waveguides ($-\eta$; blue-shaded region). In principle, one would expect to have guided modes only in the regions where the dispersion relation of the core does not overlap with that of the cladding. Indeed, we see that this is the case when we plot the spectrum of the photonics lattice (lines in Fig. 1c). To better visualize this, we colour code the spectrum: the solid blue lines represent propagating modes associated with the entire array (core + cladding), while the red lines represent the two propagating modes confined to the core region. As Fig. 1c shows, the guided modes reside around the edges of the Brillouin zone, $|k_x| = \pi/d_x$, and are non-existent around the centre of the Brillouin zone, $k_x = 0$. As expected, the spectrum is indeed asymmetric with respect to k_x, as can be understood by noticing that the symmetric guided mode (top red line in Fig. 1c) has slightly larger support in the $k_x > 0$ region of the spectrum than in the $k_x < 0$ region.

To experimentally demonstrate this guiding phenomenon we fabricated the photonic lattice sketched in Fig. 1a,b by using direct laser wiring in fused silica[50,51]. The period in x is $d_x = 16\,\mu$m, the distance between all the rows along y is $d_y = 22\,\mu$m and the tilt angle is $\eta = \pm 8\,\mu\text{m}\,\text{cm}^{-1}$. The period is $Z = d_x/\eta = 2$ cm (the same parameters as used for Fig. 1c). We fabricated two arrays, one with a core made of two rows and the other with a core made of one row only. In both cases, the total propagation distance was 10 cm. In the experiments we launch an elongated Gaussian beam, stretched in x over roughly 10–12 sites, such that it has well-defined k_x momentum. The specific value of the momentum k_x is controlled by tilting the input beam at the appropriate angle without moving the beam position itself. The input beam has a vertical width corresponding to one row, and is launched into one of the core rows. By measuring the intensity distribution at the output facet, we determine if the input beam is guided inside the core. We do so by calculating the ratio of the power within the core to the total power, measured at the output plane of the lattice, as a function of the launched wavevector k_x. The results for the array with two rows in the core are plotted in Fig. 2a, alongside simulation results using the same parameters (with a wavelength of $\lambda = 633$ nm). The experimentally measured profiles of the guiding behaviour of the array as a function of the k_x momentum are clearly shown in Supplementary Video 1. We can see that, at k_x values around the edge of the Brillouin zone, almost all of the power remains concentrated in the core—a clear indication for the existence of a guided mode at those k_x values. In contrast, at k_x values around 0, we see that almost all of the power has escaped from the core into the cladding region. Images of the light at the output facet at specific k_x values are displayed in Fig. 2b (unguided case) and Fig. 2c (guided case), where the lack of confinement (Fig. 2b) and waveguiding (Fig. 2c) of the light are clearly seen. We obtain similar results using the array with only one row in the core in Fig. 2d–f and $\lambda = 532$ nm. The experimental measurements of the guiding behaviour as a function of the k_x momentum are clearly shown in Supplementary Video 2. Again, clear evidence of guiding at k_x values around the edge of the Brillouin zone is seen both by looking at the ratio of the power at the core to the total power (Fig. 2d) for all k_x, and by examining the output beam profile at specific k_x values (Fig. 2e,f). Thus, we have experimentally demonstrated light guiding by artificial gauge fields.

Waveguiding by phase-shifted artificial gauge fields

Having demonstrated waveguiding by using different artificial gauge fields, we want to take the concept to the next level and ask 'Would it be possible to guide light in a structure where not only the core and cladding are made from the same material but where they are also subjected to the same gauge field?'

To explore this idea, we introduce a different type of gauge field and design waveguides that follow a sinusoidal trajectory. Consider an array of equidistant waveguides, where each waveguide follows a sinusoidal trajectory: $x_{\text{wg}}(z) = D\sin(\Omega z + \varphi)$. Here, Ω is the frequency of the sinusoidal modulation, D is the amplitude and φ is the phase of the modulation. One can show[30] that the equation of motion for a Bloch wave in this system is

$$i\partial_z \Phi_k(z) = 2c_1 \cos((k_x + A(z))d_x)\Phi_k(z) \tag{3}$$

where $A(z) = k_0 \dot{x}_{\text{wg}}(z) = k_0 \Omega D \cos(\Omega z + \varphi)$ is the artificial gauge field associated with the sinusoidal trajectory of the waveguides. Using the high frequency limit ($\Omega \gg c_1$), we can calculate the Floquet spectrum of equation (3) and obtain

$$\beta(k_x) = 2c_1 J_0(k_0 \Omega D d_x)\cos(k_x d_x) \tag{4}$$

where J_0 is the Bessel function of the first kind. In equation (4), we see that the effect of the gauge field is only to renormalize the coupling constant. For the special case $J_0(k_0 \Omega D d_x) = 0$, the coupling constant completely vanishes, resulting in complete localization of all wavepackets in the system. This effect is known as dynamic localization[30–34]. However, we will not use this effect here, as we wish to isolate the physics of gauge-induced waveguiding. Note that, because the average directions of the waveguides in this case coincide with the z axis, we do not have an additional additive term like in equation (2). It is important to note here that the spectrum described by equation (4) is completely independent of the phase φ of the sinusoidal trajectory of the waveguides. However, this phase can induce a non-trivial effect; for example, in Floquet topological insulators it can be used to generate topological defect modes[52,53].

Next, we constructed a waveguiding photonic lattice from arrays with sinusoidal trajectories. Consider a two-dimensional photonic lattice of such oscillating waveguides, with two rows in the middle acting as the core and the remainder acting as cladding. All the waveguides in the array follow sinusoidal trajectories with identical amplitude D and frequency Ω. The cladding waveguides have a trajectory with phase $\varphi = 0$, while the core waveguides have a trajectory with phase $\varphi = \pi$. We calculate the Floquet spectrum of such a photonic lattice by Floquet diagonalization of the continuous paraxial equation (equation (1))[47]. The spectrum is given in Fig. 3c. It immediately becomes clear that the spectrum of the modes propagating mainly in the core (red lines) is embedded within the spectrum of the cladding (blue lines). This is because, as mentioned earlier, the spectrum of an array following a sinusoidal trajectory (equation (4)) does not depend on the phase φ. Because the dispersion relations of the core and cladding are now exactly the same and therefore fully overlap, we cannot expect to find guided modes such as those presented in Fig. 1c (for the photonic lattice of tilted waveguides). Rather, waveguiding in this sinusoidal structure must rely on a fundamentally new mechanism, different from shifting the dispersion curves of the core with respect to the cladding.

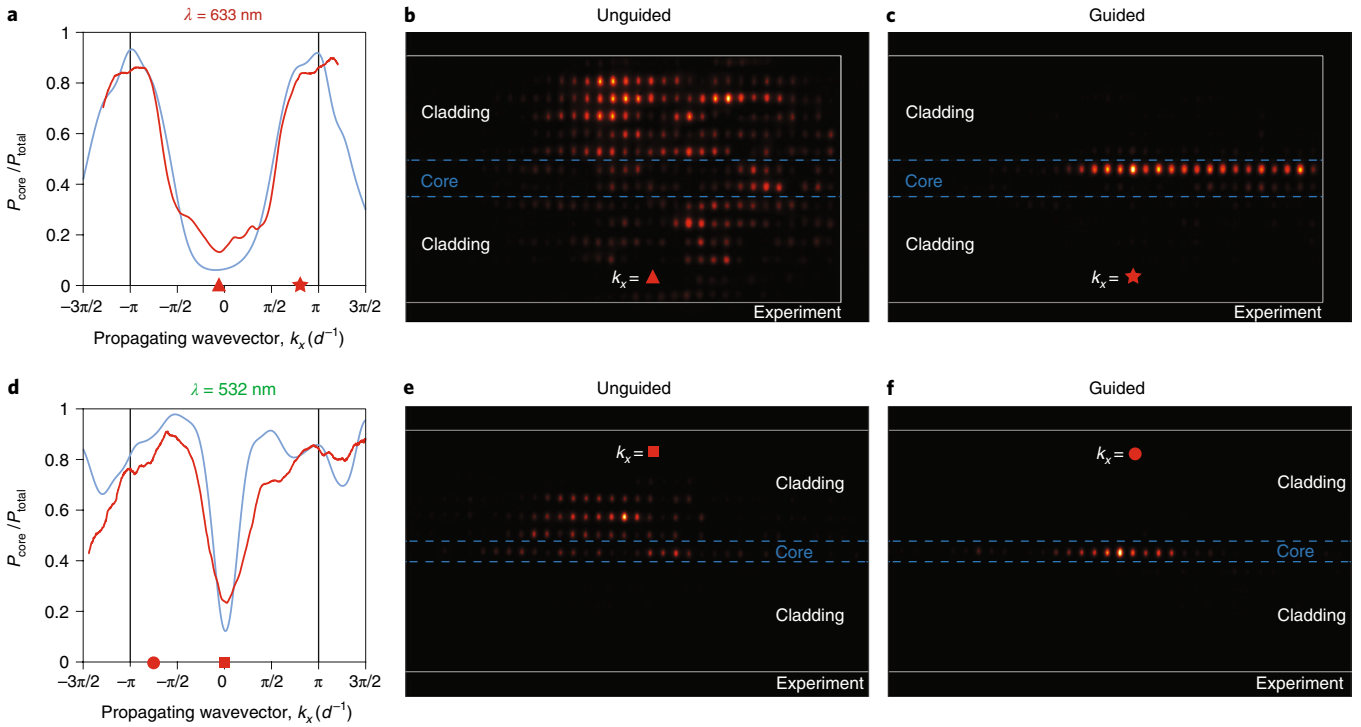

Fig. 2 | Experimental results displaying waveguiding by artificial gauge fields in tilted arrays. An elongated Gaussian beam tilted in the *x* direction is launched into one of the core arrays, such that we control its wavenumber k_x. **a**, Ratio of the power at the core to the total power measured at the output plane of the lattice, as a function of the launch wavevector k_x, as calculated in a continuum simulation (blue) and as measured in the experiment (red). **b**,**c**, Experimentally measured intensity pattern observed at the lattice output for tilt wavevector in the unguided region (**b**, k_x marked in **a** with a triangle) and in the guiding region (**c**, k_x marked in **a** as a star). **d**–**f**, Same as in **a**–**c**, but for a single-core tilted lattice.

To see the physical origin of guiding in this photonic lattice, we simplify the systems and consider just two arrays with identical gauge fields, but with different oscillation phases. That is, we consider only two adjacent arrays, a top array and a bottom array, where both arrays oscillate along a sinusoidal trajectory with the same amplitude and frequency, but at different phases. Specifically, let the top array have $\varphi = 0$, and the bottom array have $\varphi = \pi$ (Fig. 3b). Despite the fact that the two arrays have the same spectrum, the coupling between them is highly non-trivial and *z*-dependent. To achieve better understanding, we calculate the effective coupling by assuming only first-order coupling between Bloch waves (without coupling aided by crystal momentum). By also using the high frequency limit, we obtain the following approximate formula:

$$H(k_x)= \begin{pmatrix} 2c_1J_0(k_0\Omega Dd_x)\cos(k_xd_x) & c_{\mathrm{eff}}e^{-\sigma^2k_x^2/4}J_0(2k_xD) \\ c_{\mathrm{eff}}e^{-\sigma^2k_x^2/4}J_0(2k_xD) & 2c_1J_0(k_0\Omega Dd_x)\cos(k_xd_x) \end{pmatrix} \quad (5)$$

(see Supplementary Information for more details). In equation (5), $c_{\mathrm{eff}}e^{-\sigma^2k_x^2/4}$ is the effective coupling coefficient between Bloch waves of the top and bottom arrays with momentum k_x, where c_{eff} and σ are parameters we calculate numerically. According to equation (5), one can immediately see that the coupling between the two arrays vanishes at specific k_x values. This means that at values of k_x for which $J_0(2k_xD) = 0$, the top and bottom arrays are completely decoupled. At neighbouring k_x values the coupling is small, but non-zero. Intuitively, one can think of the decoupling between the core and the cladding as an interference effect from tunnelling between the two arrays, averaged over a Floquet period.

Now, going back to our full photonic lattice (Fig. 3a,b) and examining the modes of the system, we notice that there are indeed modes where the power is mostly concentrated in the core region. When we examine in detail the structure of the modes we find there are two bands of modes (red bands in Fig. 3c), which around a certain momentum region (shaded region in Fig. 3c) are strongly confined to the core. However, the decay of these confined modes into the cladding region is not exponential, as one would expect from an ordinary guided mode (a bound state in a potential well). Instead, the mode oscillates without any decay, as the mode shown in blue in Fig. 3d. This behaviour is the hallmark of leaky modes, also known as quantum resonances[54]. However, by recalling the two-array system given by equation (5) we know that, at specific k_x values, the core and the cladding are completely decoupled in the two-array system, and we expect a similar behaviour in our full photonic lattice. Indeed, there is a mode at a specific k_x value (red circle in Fig. 3c) that is perfectly confined to the core region; that is, the penetration of this specific mode into the cladding is identically zero, as shown in red in Fig. 3d. If we plot, as a function of k_x, the ratio of the peak intensity in the core of these leaky modes to the mean intensity in the cladding, we find a sharp peak corresponding to $J_0(2k_xD) = 0$, where the core and the cladding are completely decoupled (see Supplementary Information). This resonant behaviour means that this mode is a BIC. Conventionally, BICs are bound modes whose energy is embedded in the continuum part of the spectrum, but they are nevertheless forbidden from coupling to the continuum modes due to symmetries[41–44] or through parameter tuning that completely suppresses coupling to radiating modes[44,45]. Here, we show that our guided mode corresponds to a dynamic BIC[43], which has never been demonstrated in experiments.

To experimentally demonstrate this new guiding phenomenon, we fabricated the photonic lattice of Fig. 3a by using direct laser

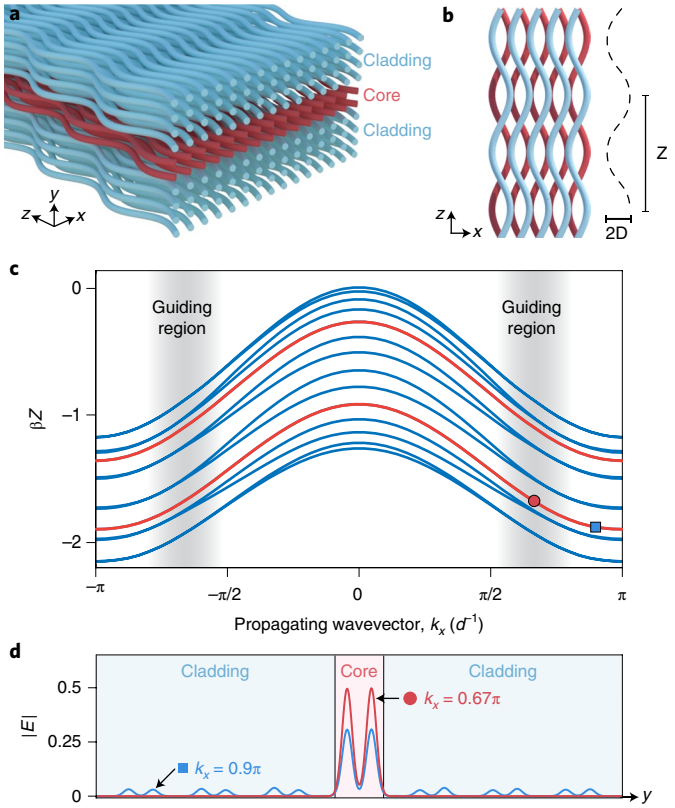

Fig. 3 | Waveguiding of light by phase-shifted but otherwise identical artificial gauge fields. a,**b**, Schematic of the two-dimensional waveguide array of sinusoidal trajectories showing guiding by phase-shifted artificial gauge fields. All the waveguides are identical and follow a sinusoidal trajectory with the same periodicity and amplitude, but the cladding (blue) and core (red) rows are π-phase shifted. **c**, Dispersion of the waveguide array depicted in **a**. The blue lines represent extended modes over the whole array, while the red lines represent modes confined to the core. **d**, Amplitude profiles for two of the modes (red circle and blue square in **c**) that are mostly confined to the core. The red profile shows the special mode that has zero coupling to the cladding (exemplified by the zero energy in the cladding). For comparison, we plot a mode at a different k_x value (blue), where the leakage into the cladding is evident.

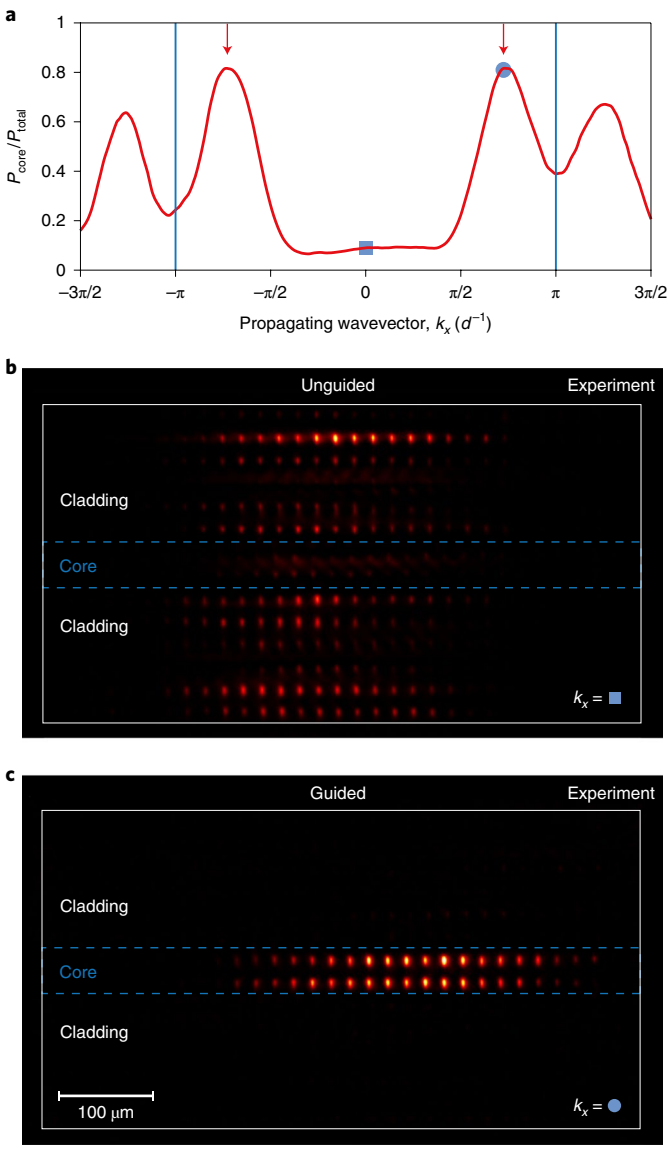

Fig. 4 | Experimental results displaying waveguiding by phase-shifted artificial gauge fields. We launch, into both of the core arrays, an elongated Gaussian beam tilted in the *x* direction such that we control its wavenumber k_x. The lattice oscillation amplitude is 8 μm. **a**, Ratio of the power at the core to the total power in the array, measured at the output plane of the lattice, as a function of the launch wavevector, k_x. Red arrows mark the position of maximum core guiding calculated by the continuum simulation, which clearly agrees with the experimental results. Blue vertical lines mark the Brillouin zone (notice the expected peak replicas outside the Brillouin zone). **b**,**c**, Experimentally observed intensity profiles at the lattice output for a propagating wavevector in the unguided region (**b**) (k_x marked in **a** with a square) and in the guiding region (**c**) (k_x marked in **a** as a circle).

wiring in fused silica[50,51]. The period in x is $d_x = 20\,\mu m$, the distance between the arrays along y is $d_y = 24\,\mu m$, the frequency is $\Omega = 2\pi\,rad\,cm^{-1}$ and the amplitude is $D = 8\,\mu m$ (the same parameters as used in Fig. 3c). We launch an elongated Gaussian beam with well-defined k_x into the core, and measure the ratio of the power within the core to the total power measured at the output plane of the lattice. The results are plotted in Fig. 4a, which shows two peaks at $k_x = 0.73\pi/d_x$, clearly demonstrating that the core of our photonic lattice is guiding light at a specific value of momentum. Notice that the expected peak positions from continuum simulations (arrows in Fig. 4a) are in perfect agreement with our measurements. The resonant nature of the guiding mechanism can clearly be observed at the measured beam profile at the output facet for a k_x corresponding to maximum guiding (Fig. 4c) and for a k_x where there is no guiding (Fig. 4b). The experimental measurements of the guiding behaviour as a function of the k_x momentum over the entire Brillouin zone are clearly shown in Supplementary Video 3. We note that in Fig. 4a the two peaks do not reach perfect confinement (unity) because the initial excitation at the core is a Gaussian wavepacket instead of a Bloch mode, which causes a fraction of the input beam to couple to higher bands.

To fully characterize this phenomenon, we designed a set of experiments to measure how the position of maximum guiding (the BIC's position) is affected by changing the amplitude D of the sinusoidal trajectory. According to our approximation in equation (5), the peak position should be decreasing with increasing D. To corroborate this, we fabricated three photonic lattices with sinusoidal amplitudes $D = 6\,\mu m$, $8\,\mu m$ and $10\,\mu m$, respectively. We again launch an elongated Gaussian beam with well-defined k_x into the core and measure the ratio of power at the core, and the results are shown in Fig. 5. We clearly see that the position of the peak where the

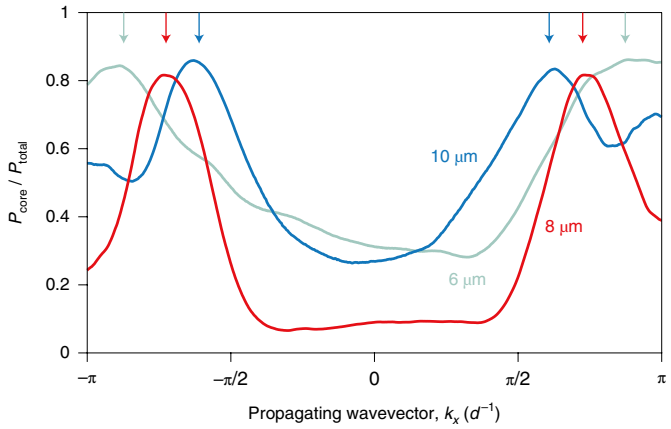

Fig. 5 | Experimental results displaying phase-shifted gauge guiding in sinusoidal arrays. We launch an elongated Gaussian beam ($\lambda = 633$ nm) into one of the core rows and scan its tilt angles in the x direction, thereby scanning the k_x momentum component. The figure shows the experimentally measured ratio of the power in the core to the total power in the array, measured at the output plane of the lattice, as a function of the launched wavevector, k_x, for three different lattices with different oscillation amplitudes: 6 μm (green), 8 μm (red) and 10 μm (blue). Notice how the peak position of the guided power moves to smaller $|k_x|$ as we increased the oscillation amplitude of the array. The arrows mark the positions of maximum core guiding calculated by the continuum simulation, which clearly agree with the experimental results.

guiding occurs (that is, the BIC position) decreases for lattices with increasing sinusoidal amplitude D, as we predicted from our theoretical analysis. Our experimental results also match very well the full-wave continuum simulations, as marked by the arrows in Fig. 5. These new waveguiding mechanism can be used as a transverse momentum; by propagating a wavepacket in our photonic lattice we can filter a specific momentum component by only coupling to the core of the system. Altogether, the experimental results (Figs. 4 and 5) demonstrate a new gauge-induced waveguiding mechanism, where the core and the cladding regions are made from the same material and are subjected to the same artificial gauge fields characterized by the same dispersion curves, with the only difference being a phase shift in the dynamics of the gauge field. Waveguiding of this sort relates to BICs, quantum resonances and dynamic localization and offers a new platform for engineering these phenomena by making use of artificial gauge fields.

Conclusions

In summary, we have experimentally demonstrated the phenomenon of guiding light by virtue of artificial gauge fields. We fabricated photonic lattices where artificial gauge fields induce different dispersion relations at the core and cladding regions, and observed how this gives rise to guided modes. In a more advanced setting, we have demonstrated how to induce waveguiding by only changing the phase of the gauge field, while the dispersion curves of the core and cladding are identical. We have shown that, in such settings, the guiding occurs because the interaction between the core and the cladding is non-trivial and can lead to nulling the coupling altogether, which offers precise control over the momentum values at which the guiding takes place. The principles of our waveguiding mechanism can also be implemented in systems that break time-reversal symmetry, such as the time-modulated resonators described in ref. [11]. By changing or modulating the system around the resonant frequency, it is possible to emulate the phenomenon of waveguiding via phase-shifted artificial gauge fields. The new guiding mechanisms demonstrated here open the door to new applications of artificial gauge fields in photonics, and by their fundamental nature are applicable not only to the entire electromagnetic spectrum and different optical systems, but also to other physical systems such as acoustics and cold atoms.

Online content

Any methods, additional references, Nature Research reporting summaries, source data, statements of data availability and associated accession codes are available at https://doi.org/10.1038/s41566-019-0370-1.

Received: 26 July 2018; Accepted: 25 January 2019;
Published online: 11 March 2019

References

1. Snyder, A. W. & Love, J. *Optical Waveguide Theory* (Springer, 1983).
2. Yeh, P. & Yariv, A. Bragg reflection waveguides. *Opt. Commun.* **19**, 427–430 (1976).
3. Ibanescu, M., Fink, Y., Fan, S., Thomas, E. L. & Joannopoulos, J. D. An all-dielectric coaxial waveguide. *Science* **289**, 415–419 (2000).
4. Russell, P. Photonic crystal fibers. *Science* **299**, 358–362 (2003).
5. Knight, J. C. Photonic crystal fibres. *Nature* **424**, 847–851 (2003).
6. Joannopoulos, J. D., Johnson, S. G., Winn, J. N. & Meade, R. D. *Photonic Crystals: Molding the Flow of Light* (Princeton Univ. Press, 2008).
7. Yariv, A., Xu, Y., Lee, R. K. & Scherer, A. Coupled-resonator optical waveguide: a proposal and analysis. *Opt. Lett.* **24**, 711–713 (1999).
8. Cohen, O., Freedman, B., Fleischer, J. W., Segev, M. & Christodoulides, D. N. Grating-mediated waveguiding. *Phys. Rev. Lett.* **93**, 103902 (2004).
9. Alberucci, A., Marrucci, L. & Assanto, G. Light confinement via periodic modulation of the refractive index. *New J. Phys.* **15**, 083013 (2013).
10. Slussarenko, S. et al. Guiding light via geometric phases. *Nat. Photon.* **10**, 571–575 (2016).
11. Lin, Q. & Fan, S. Light guiding by effective gauge field for photons. *Phys. Rev. X* **4**, 031031 (2014).
12. Madison, K. W., Chevy, F., Wohlleben, W. & Dalibard, J. Vortex formation in a stirred Bose–Einstein condensate. *Phys. Rev. Lett.* **84**, 806–809 (2000).
13. Lin, Y.-J., Compton, R. L., Jiménez-García, K., Porto, J. V. & Spielman, I. B. Synthetic magnetic fields for ultracold neutral atoms. *Nature* **462**, 628–632 (2009).
14. Rechtsman, M. C. et al. Photonic Floquet topological insulators. *Nature* **496**, 196–200 (2013).
15. Hafezi, M., Mittal, S., Fan, J., Migdall, A. & Taylor, J. M. Imaging topological edge states in silicon photonics. *Nat. Photon.* **7**, 1001–1005 (2013).
16. Lustig, E. et al. Photonic topological insulator in synthetic dimensions. *Nature* https://doi.org/10.1038/s41586-019-0943-7 (2019).
17. Jotzu, G. et al. Experimental realization of the topological Haldane model with ultracold fermions. *Nature* **515**, 237–240 (2014).
18. Aidelsburger, M. et al. Measuring the Chern number of Hofstadter bands with ultracold bosonic atoms. *Nat. Phys.* **11**, 162–166 (2014).
19. Schmidt, M., Kessler, S., Peano, V., Painter, O. & Marquardt, F. Optomechanical creation of magnetic fields for photons on a lattice. *Optica* **2**, 635–641 (2015).
20. Xiao, M., Chen, W.-J., He, W.-Y. & Chan, C. T. Synthetic gauge flux and Weyl points in acoustic systems. *Nat. Phys.* **11**, 920–924 (2015).
21. Fleury, R., Khanikaev, A. B. & Alù, A. Floquet topological insulators for sound. *Nat. Commun.* **7**, 11744 (2016).
22. Süsstrunk, R. & Huber, S. D. Observation of phononic helical edge states in a mechanical topological insulator. *Science* **349**, 47–50 (2015).
23. Nash, L. M. et al. Topological mechanics of gyroscopic metamaterials. *Proc. Natl Acad. Sci. USA* **112**, 14495–14500 (2015).
24. Umucalılar, R. O. & Carusotto, I. Artificial gauge field for photons in coupled cavity arrays. *Phys. Rev. A* **84**, 043804 (2011).
25. Hafezi, M., Demler, E. A., Lukin, M. D. & Taylor, J. M. Robust optical delay lines with topological protection. *Nat. Phys.* **7**, 907–912 (2011).
26. Fang, K., Yu, Z. & Fan, S. Realizing effective magnetic field for photons by controlling the phase of dynamic modulation. *Nat. Photon.* **6**, 782–787 (2012).
27. Longhi, S. Effective magnetic fields for photons in waveguide and coupled resonator lattices. *Opt. Lett.* **38**, 3570–3573 (2013).
28. Rechtsman, M. C. et al. Strain-induced pseudomagnetic field and photonic Landau levels in dielectric structures. *Nat. Photon.* **7**, 153–158 (2013).
29. Cheng, X. et al. Robust reconfigurable electromagnetic pathways within a photonic topological insulator. *Nat. Mater.* **15**, 542–548 (2016).
30. Dunlap, D. H. & Kenkre, V. M. Dynamic localization of a charged particle moving under the influence of an electric field. *Phys. Rev. B* **34**, 3625–3633 (1986).

31. Longhi, S. et al. Observation of dynamic localization in periodically curved waveguide arrays. *Phys. Rev. Lett.* **96**, 243901 (2006).
32. Garanovich, I. L. et al. Diffraction control in periodically curved two-dimensional waveguide arrays. *Opt. Express* **15**, 9737–9747 (2007).
33. Szameit, A. et al. Polychromatic dynamic localization in curved photonic lattices. *Nat. Phys.* **5**, 271–275 (2009).
34. Szameit, A. et al. Observation of two-dimensional dynamic localization of light. *Phys. Rev. Lett.* **104**, 223903 (2010).
35. Li, E., Eggleton, B. J., Fang, K. & Fan, S. Photonic Aharonov–Bohm effect in photon–phonon interactions. *Nat. Commun.* **5**, 3225 (2014).
36. Tzuang, L. D., Fang, K., Nussenzveig, P., Fan, S. & Lipson, M. Non-reciprocal phase shift induced by an effective magnetic flux for light. *Nat. Photon.* **8**, 701–705 (2014).
37. Fang, K. & Fan, S. Controlling the flow of light using the inhomogeneous effective gauge field that emerges from dynamic modulation. *Phys. Rev. Lett.* **111**, 203901 (2013).
38. Yuan, L., Shi, Y. & Fan, S. Photonic gauge potential in a system with a synthetic frequency dimension. *Opt. Lett.* **41**, 741–744 (2016).
39. Harari, G. et al. Topological insulator laser: theory. *Science* **359**, eaar4003 (2018).
40. Bandres, M. A. et al. Topological insulator laser: experiments. *Science* **359**, eaar4005 (2018).
41. Plotnik, Y. et al. Experimental observation of optical bound states in the continuum. *Phys. Rev. Lett.* **107**, 183901 (2011).
42. Hsu, C. W. et al. Observation of trapped light within the radiation continuum. *Nature* **499**, 188–191 (2013).
43. Longhi, S. & Valle, G. D. Floquet bound states in the continuum. *Sci. Rep.* **3**, 2219 (2013).
44. Hsu, C. W., Zhen, B., Stone, A. D., Joannopoulos, J. D. & Soljačić, M. Bound states in the continuum. *Nat. Rev. Mater.* **1**, 16048 (2016).
45. Zhen, B., Hsu, C. W., Lu, L., Stone, A. D. & Soljačić, M. Topological nature of optical bound states in the continuum. *Phys. Rev. Lett.* **113**, 257401 (2014).
46. Lederer, F. et al. Discrete solitons in optics. *Phys. Rep.* **463**, 1–126 (2008).
47. Plotnik, Y. et al. Analogue of Rashba pseudo-spin–orbit coupling in photonic lattices by gauge field engineering. *Phys. Rev. B* **94**, 020301(R) (2016).
48. Mazor, Y., Hadad, Y. & Steinberg, B. Z. Planar one-way guiding in periodic particle arrays with asymmetric unit cell and general group-symmetry considerations. *Phys. Rev. B* **92**, 125129 (2015).
49. El-Ganainy, R. & Levy, M. Optical isolation in topological-edge-state photonic arrays. *Opt. Lett.* **40**, 5275–5278 (2015).
50. Szameit, A. & Nolte, S. Discrete optics in femtosecond-laser-written photonic structures. *J. Phys. B At. Mol. Opt. Phys.* **43**, 163001 (2010).
51. Heinrich, M. et al. Supersymmetric mode converters. *Nat. Commun.* **5**, 3698 (2014).
52. Tenenbaum Katan, Y. & Podolsky, D. Generation and manipulation of localized modes in Floquet topological insulators. *Phys. Rev. B* **88**, 224106 (2013).
53. Tenenbaum Katan, Y. & Podolsky, D. Modulated Floquet topological insulators. *Phys. Rev. Lett.* **110**, 016802 (2013).
54. Moiseyev, N. Quantum theory of resonances: calculating energies, widths and cross-sections by complex scaling. *Phys. Rep.* **302**, 212–293 (1998).

Acknowledgements

This work was supported by the German–Israeli DIP Program (grant no. BL 574/13-1), the United States Air Force Office of Scientific Research, the Deutsche Forschungsgemeinschaft (grants nos. SZ 276/9-1, SZ 276/19-1 and SZ 276/20-1) and an Advanced Grant from the European Research Council. The authors thank C. Otto for preparing the high-quality fused-silica samples used in all experiments presented here.

Author contributions

All authors contributed significantly to this work.

Competing interests

The authors declare no competing interests.

Additional information

Supplementary information is available for this paper at https://doi.org/10.1038/s41566-019-0370-1.

Reprints and permissions information is available at www.nature.com/reprints.

Correspondence and requests for materials should be addressed to M.S.

Publisher's note: Springer Nature remains neutral with regard to jurisdictional claims in published maps and institutional affiliations.

Methods

Fabrication. We fabricated the waveguides in 10 cm fused-silica glass (Corning 7980) samples by using the femtosecond laser writing method[50]. We used pulses created by a Coherent RegA 9000 amplifier seeded with a Coherent Mira 900 Ti:sapphire laser that have an energy of 450 nJ at 800 nm and 100 kHz. An Aerotech ALS 130 direct-drive linear stage together with a microscope objective (0.35 numerical aperture) provided highly accurate focusing of the laser beam from 50 μm to 800 μm under the sample surface. By moving the sample with a speed of 100 mm min^{-1} the refractive index at the focal point was changed around 7×10^{-4}. This created waveguides with a mode field diameter of 10.4 μm × 8 μm at 632.8 nm. Propagation losses and birefringence were estimated to be 0.2 dB cm^{-1} and 1×10^{-7}, respectively. A table including all the parameters and microscope images of the fabricated optical lattices are provided in the Supplementary Information.

Experimental set-up. We generated an elongated Gaussian beam (~130–190 μm x -width and ~8–12 μm y width at $\lambda=633$ nm and 532 nm) at the input facet of the waveguide array by taking the Fourier transform of a rectangular slit using a single achromatic lens. The position of the slit (Fourier plane of the elongated Gaussian beam) was scanned in the x direction (~10 μm per step) by using a stepper motor to scan the phase of the input beam, which was translated into scanning the k_x of the Bloch mode launched into the photonic lattice. This allowed us to collect up to ~800 measurements inside the Brillouin zone. The light intensity distribution at the output facet of the array was imaged onto a linear CMOS camera (1,920 × 1,200 pixels, 1/12-inch sensor) by using ×10 and ×20 objectives. The size of the Brillouin zone (or the k_x momentum step) was calculated using geometric optics and by correlating the output profiles.

Simulations. All the simulation results were obtained from full continuum simulations of the paraxial wave equation with the corresponding lattice refractive index profile. Each waveguide was modelled as a super-Gaussian profile given by $\Delta n=\Delta n_0\exp(-(x/w_x)^6-(y/w_y)^6)$ with $w_x=1.9$ μm, $w_y=5.5$ μm and $\Delta n_0=7.5\times10^{-4}$. The background refractive index was $n_0=1.45$. These parameters were estimated from the output profile of single, one-dimensional and two-dimensional arrays of straight waveguides that were fabricated together with the lattices study here. The continuum Floquet band structure and eigenmodes presented in Figs. 1c and 3c,d were calculated using a continuum Floquet eigensolver, as described in the supplementary information of ref. [47].

Data availability

The data that support the plots within this paper and other findings of this study are available from the corresponding authors upon reasonable request.